MANCHESTER 1824
The University of Manchester

The University of Manchester Research

Effects of inertia distribution on regional frequency heterogeneity

DOI:
10.1016/j.epsr.2024.110340

Document Version
Final published version

Link to publication record in Manchester Research Explorer

Citation for published version (APA):
Zhang, Z., & Preece, R. (2024). Effects of inertia distribution on regional frequency heterogeneity. *Electric Power Systems Research*, *231*(110340). https://doi.org/10.1016/j.epsr.2024.110340

Published in:
Electric Power Systems Research

Citing this paper
Please note that where the full-text provided on Manchester Research Explorer is the Author Accepted Manuscript or Proof version this may differ from the final Published version. If citing, it is advised that you check and use the publisher's definitive version.

General rights
Copyright and moral rights for the publications made accessible in the Research Explorer are retained by the authors and/or other copyright owners and it is a condition of accessing publications that users recognise and abide by the legal requirements associated with these rights.

Takedown policy
If you believe that this document breaches copyright please refer to the University of Manchester's Takedown Procedures [http://man.ac.uk/04Y6Bo] or contact uml.scholarlycommunications@manchester.ac.uk providing relevant details, so we can investigate your claim.

OPEN ACCESS

Download date:18. May. 2024

Electric Power Systems Research 231 (2024) 110340

Contents lists available at ScienceDirect

Electric Power Systems Research

journal homepage: www.elsevier.com/locate/epsr

Effects of inertia distribution on regional frequency heterogeneity

Zaichun Zhang *, Robin Preece

Department of Electrical and Electronic Engineering, The University of Manchester, Manchester, UK

ARTICLE INFO

Keywords:
Electromechanical oscillations
Fast frequency response
Frequency containment
Heterogeneity
Inertia distribution

ABSTRACT

Heterogeneous inertia distribution can result in large regional frequency deviations and inter-area oscillations that exceed protection limits configured based on system-wide averaged performance. This paper examines how the spatial distribution of inertia affects frequency heterogeneity. Along with varying inertia distribution, variations in generator turbine-governor control and network topology are studied to make the results more generalisable across wide-ranging operating conditions. An investigation into the effects of different fast frequency response (FFR) schemes on frequency heterogeneity is also presented. The frequency heterogeneity is quantified by calculating cosine similarity between regional frequency trajectories. The key results are obtained using a two-area model and verified using a mixed AC/DC power system. A key finding is that the localness of regional frequency is independent of the inertia of a specific area, nor of the total system inertia. The inertia ratio, described as the ratio of the disturbance area inertia to that of the non-disturbance area, is shown to have a strong correlation with frequency heterogeneity. This correlation is shown to be very robust to changes in generator dynamics and network topology. Providing derivative FFR within the disturbance area always demonstrates benefits regarding frequency heterogeneity inhibition, whereas droop scheme typically introduces deterioration in frequency heterogeneity.

1. Introduction

Frequency stability has typically been studied using equivalent system models. Dynamics of all synchronous generators (SGs) are considered to be coherent during transients, represented by the centre of inertia (COI) frequency [1]. As converter interfaced generation (CIG) proliferates, the quantity of stored synchronous kinetic energy (i.e., *inertia*) within the system will no longer be a global variable and is instead heterogeneous, subjected to generation location and network topology [1]. Consequently, the frequency experienced around the network will vary considerably between areas following disturbances. Areas that exhibit relatively low levels of inertia will experience faster change of frequency deviation and larger angular divergence with respect to neighbouring areas, leading to substantial power oscillations across inter-area ties [2]. System operators will therefore experience difficulties with regional- and system-wide stability containment. This has encouraged research specifically concerned with the stability issues induced by heterogeneous inertia distribution.

Studies [3–5] are conducted using small (two- or three-area) test networks. An early study into the effects that large differences in regional inertia have on angle stability is presented in [3]. Increased angular separation between areas is shown when disturbances occur close to the low inertia area. The authors in [4,5] explore how inter-area oscillations are affected by inertia distribution. It shows that in the presence of heterogeneous inertia distribution, fast and large flows of power will be transferred between areas. There are also studies attempting to examine the effects of inertia distribution on large multi-area networks, as in [6–9]. A 16-machine 68-bus network is used in [6] for probabilistic frequency stability studies, highlighting the limitations of using equivalent models in representing distinct locational frequencies. By using a reduced order Great Britain (GB) network, frequency stability assessment under varying regional inertia distributions is carried out in [7]. This work identifies protection issues induced by heterogeneous inertia distribution. In [8], a synthetic Texas system is used for frequency stability studies. It highlights that local or regional rate of change of frequency (ROCOF) can vary significantly from system-wide ROCOF when the system exhibits inertia heterogeneity. A method based on spectral clustering is developed in [9] which can be used to identify regions that are vulnerable to issues induced by inertia heterogeneity.

Implementing fast frequency response (FFR) to mitigate the stability issues induced by inertia heterogeneity has received recent attention. FFR schemes are usually designed to deliver large quantities of active power within milliseconds to a few seconds following disturbances. Both *droop* response and *synthetic inertia* can be provided from the FFR devices, dependent on the control schemes applied [10]. With performance metrics as objectives, the problem has often been formulated

* Corresponding author.
E-mail address: zaichun.zhang@manchester.ac.uk (Z. Zhang).

https://doi.org/10.1016/j.epsr.2024.110340
Received 22 March 2023; Accepted 18 March 2024
0378-7796/© 2024 The Author(s). Published by Elsevier B.V. This is an open access article under the CC BY license (http://creativecommons.org/licenses/by/4.0/).

as optimisation problems such as eigenvalue sensitivity-based optimisation [5,11] and system norms minimisation ($\mathcal{H}_2$, $\mathcal{L}_2$, $\mathcal{L}_\infty$) [12,13]. However, no consensus has been reached as the results vary (sometimes conflicting) according to the performance metrics being used. Also, these approaches may fail to reflect dynamics during large system transients whilst using linearised forms of the system model to ascertain optimised solutions.

Although studies to date have recognised regional variations in frequency, a systematic understanding of how inertia distribution contributes to frequency heterogeneity is still lacking. Further, there has been no quantitative analysis of the extent to which inertia distribution determines the *localness* of regional frequency. The way in which different FFR schemes affect frequency heterogeneity is not well understood and requires further investigation.

This paper presents a comprehensive investigation into the effects of inertia distribution on frequency heterogeneity. The knowledge gained would help in safely resourcing inertia and FFR services in low inertia systems. Significantly, it lays the groundwork for future research into the determination of regional inertia floors and regional FFR implementation requirements. The main contributions of this paper are:

1. The identification of a new measure of inertia distribution to characterise frequency heterogeneity.
2. The determination of the relationship between inertia distribution and frequency heterogeneity.
3. An explanation of the way in which frequency heterogeneity is affected by different FFR control schemes.

2. Theoretical background

A common equation for describing rotor dynamics of SG is the *swing equation* as given by (1)–(3), where ω and $\Delta\omega$ are the speed and speed deviation in rad/s, ω_{syn} is the synchronous speed in rad/s, τ_m and τ_e are the mechanical and electrical torque in per unit (pu), τ_{net} refers to the net torque in pu, P_m and P_e are the mechanical and electrical power in pu, H is the inertia constant in seconds, and δ is the rotor angle in radians.

$$\tau_m = \frac{P_m}{\omega}; \tau_e = \frac{P_e}{\omega} \tag{1}$$

$$\frac{d}{dt}\Delta\omega = \frac{\omega_{syn}}{2H}(\tau_m - \tau_e) = \frac{\omega_{syn}}{2H}\tau_{net} \tag{2}$$

$$\frac{d}{dt}\delta = \Delta\omega = \omega - \omega_{syn} \tag{3}$$

Looking at (2) highlights that both H and τ_{net} are underlying factors in determining frequency deviation at a specific location (or a region) during transient events. In a multi-area network, not only does each area store a specific amount of inertial energy, but the τ_{net} experienced after disturbances is also different. This explains the reason why variations in regional frequency are seen across the network at the initial phase of a disturbance. The unique oscillatory behaviour of the regional frequency means that SGs (or groups of SGs) are not accelerating (or decelerating) together. This gives rise to angular divergence between areas and power oscillations across inter-area ties. The spatial distribution of inertia across the system changes with the variation in regional generation mix during unit commitment processes. As a result, the oscillatory behaviour of the regional frequency and hence the electromechanical interactions between regions following a disturbance will be altered, which ultimately leads to differences in frequency heterogeneity. The next section will present a methodology that can be used to explore the extent to which the inertia distribution affects frequency heterogeneity.

3. Methodology

This paper investigates the effects of inertia distribution on frequency heterogeneity by performing phasor based simulations. This involves a large number of simulations where each simulation is created from a unique combination of regional inertia distributions in the system. For each simulation a metric that measures frequency heterogeneity is determined. To examine the relationship between inertia-based variables and frequency heterogeneity, correlation analysis is conducted. The procedure used to complete the investigation is outlined in Fig. 1, with further details elaborated on in the following subsections.

Generic frequency heterogeneity investigation procedure	
Inputs:	Phasor-based power system models.
Step 1	Create distinct inertia distributions.
Step 2	Select a measure that can quantify frequency heterogeneity.
Step 3	Run simulations and calculate the measure of frequency heterogeneity.
Step 4	Conduct correlation analysis.
Outputs:	Inertia-based variables, the measure of frequency heterogeneity, correlation coefficient.

Fig. 1. Frequency heterogeneity investigation procedure.

3.1. Distinct inertia distributions creation (step 1)

Strictly speaking, any power sources and loads that exhibit some active power deviations after a disturbance would contribute to the inertial response of the power system [14]. In this study, only the inertial contribution from the SGs is considered as it typically contributes most of the inertial response. The stored synchronous inertial energy within the SGs (E_{syn}) is given by (4), where S is the machine rating in VA, and $\mathcal{G}$ is the number of committed SG units within a pre-determined region.

$$E_{syn} = \sum_{g=1}^{\mathcal{G}} H_g S_g \tag{4}$$

Different levels of regional (and hence system) inertia are typically created by changing system loading and then rescheduling SGs. In this study, this is achieved by adjusting the H values of the SGs in each region. This allows simple but precise variations in regional inertia, making it particularly useful for producing wide ranging system conditions with respect to inertia distribution. Such a way in which distinct inertia distributions are created was also considered in studies [15,16].

3.2. Frequency heterogeneity quantification (step 2)

Quantification of frequency heterogeneity is needed in order to perform a systematic investigation into the impact of inertia distribution. In essence, to quantify frequency heterogeneity is to measure the *similarity* between frequency trajectories. Several methods currently exist for the measurement of trajectory similarity such as Euclidean distance, Hausdorff distance, cosine similarity, and Jaccard similarity [17]. In this research, *cosine similarity* is used as it is particularly useful for capturing and characterising oscillatory behaviour between trajectories.

Cosine similarity (CS) is defined as the cosine of the angle between vectors through the inner product [17]. A set of regional frequency trajectories of a network with M pre-determined regions can be described as $\mathbf{F} = \{\mathbf{F_1}, \mathbf{F_i}, \ldots, \mathbf{F_M}\}$. $\mathbf{F_i}$ is a $1 \times N$ vector and can be described as $\{f_{i,1}, f_{i,n}, \ldots, f_{i,N}\}$, in which N is the number of sampling points. The CS between the frequency of i-th and j-th region is defined as

$$\mathrm{CS_{ij}} = \frac{1}{N-1}\sum_{n=2}^{N-1} \frac{\overrightarrow{f_{i,n}f_{i,n+1}}\,\overrightarrow{f_{j,n}f_{j,n+1}}}{\left\|\overrightarrow{f_{i,n}f_{i,n+1}}\right\|\left\|\overrightarrow{f_{j,n}f_{j,n+1}}\right\|} \tag{5}$$

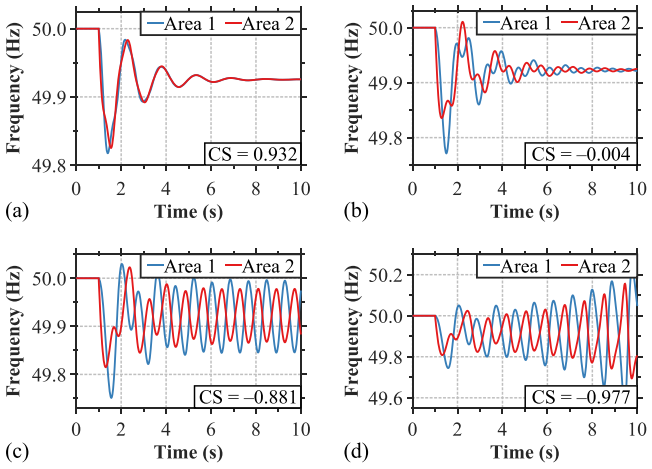

Fig. 2. Examples of regional frequency trajectories for different CS values: (a) highly synchronous; (b) moderate oscillation; (c) poorly damped stable oscillation; (d) significant oscillation.

The value of CS is bounded in the range [–1, 1]. The closer CS is to 1, the more similar the two trajectories are. In the context of synchronous operation, a CS value close to 1 indicates that SGs (or groups of SGs) are highly synchronous during transients. Conversely, a CS value close to –1 means that SGs are significantly oscillating against each other. Fig. 2 displays four pairs of typical regional frequency trajectories that lead to different values of CS. The results are generated using a two-area network which will be elaborated on further in Section 4.2.

Considering all possible combinations of comparison between two regional frequency trajectories, a matrix of the values of CS of an M-area network can be constructed, as given in (6)

$$\mathbf{CS} = \begin{bmatrix} \mathrm{CS}_{11} & \cdots & \mathrm{CS}_{1i} & \cdots & \mathrm{CS}_{1M} \\ \vdots & \ddots & \vdots & & \vdots \\ \mathrm{CS}_{i1} & \cdots & \mathrm{CS}_{ii} & \cdots & \mathrm{CS}_{iM} \\ \vdots & & \vdots & \ddots & \vdots \\ \mathrm{CS}_{M1} & \cdots & \mathrm{CS}_{Mi} & \cdots & \mathrm{CS}_{MM} \end{bmatrix} \tag{6}$$

The matrix **CS** is an $M \times M$ matrix with diagonal entries all one (i.e., $\mathrm{CS}_{ii} = 1$). Also, the entries of the matrix are symmetric with respect to the main diagonal (i.e., $\mathrm{CS}_{ij} = \mathrm{CS}_{ji}$). In this study, the *arithmetic mean* of the sum of the upper triangular portion of the **CS** matrix (excluding the main diagonal but including all entries above it) is used to quantify frequency heterogeneity. For example, for a four-area network, six combinations of comparison between two areas can be drawn to calculate the CS: CS_{12}, CS_{13}, CS_{14}, CS_{23}, CS_{24}, and CS_{34}. The frequency heterogeneity is quantified by calculating the arithmetic mean of the six CS values. Note that the frequency heterogeneity of a two-area network can directly be quantified using (5), which is equal to CS_{12} in the corresponding **CS** matrix.

3.3. Simulation and data collection (step 3)

Throughout this study, the signal of rotor speed is used to represent generator frequency dynamics. The speed deviations are initiated by a sudden disconnection of an extra static generator that does not possess any inertia or dynamic properties at the target location. In this way, the pre- and post-disturbance values of E_{syn} in the system are identical, compared to when SG tripping is implemented.

Assessing all combinations of regional inertia leads to a large number of simulations. The length of the simulation is 10 s long with the disturbance occurring at 1 s. The sample size of 10 ms is selected — in total 900 sampling points for each speed trajectory. For each simulation, the CS between each pair of speed trajectories is calculated using (5). After arranging the resulting CS values into a matrix as in (6), the system averaged CS is calculated. A multivariate data set, including inertia-based variables and the averaged CS values for all cases, is then created which will be used in correlation analysis.

3.4. Correlation analysis (step 4)

Correlation analysis is performed to ascertain whether inertia-based variables and the measure of frequency heterogeneity (values of system averaged CS in this case) are *linearly* related. This helps determine the relationship between inertia distribution and frequency heterogeneity. To quantify the strength of linear relationships, the Pearson correlation coefficient (ρ) as given in (7) is used, in which Cov(·) is the covariance between variables and σ is the variable standard deviation [18]. Interpretation of the magnitude of ρ can be found in [18].

$$\rho_{xy} = \frac{\mathrm{Cov}(x, y)}{\sigma_x \sigma_y} \tag{7}$$

3.5. Changes in system dynamics and topology (inputs)

The results from simulation based approaches are intrinsically bespoke and highly dependent on the properties of the systems and components modelled [1]. To enable the generalisability of the results, a scenario-based analysis should be conducted during the investigation. Also, performing the analysis on different systems establishes the robustness of the key findings to topological and system dynamics alterations. To conduct a comprehensive assessment into the impact of inertia distribution on frequency heterogeneity, variations in network factors, including SG turbine-governor control and network topology, are considered in this research. These studies are completed by initialising the system setups (i.e., Inputs, Fig. 1) one at a time on the basis of specific network factors of interest.

Regarding the generator turbine-governor control, variations in governor droop (R) and governor control model are of particular interest. The values of R typically lie in the range [3, 9]% [19]. The type of machine and turbine-governor model employed depends on the working fluid (such as steam, gas, and hydraulic) that is provided to the turbine [20].

Regarding the network topology, variations in *shortest path length* and *network connectedness* are of interest. Shortest path length is known as *shortest distance* in graph theory, which refers to the shortest network distance between two vertices in a graph [21]. In the context of power systems, it is the *electrical distance* (i.e., the Thévenin impedance [22]) between two buses within a network. Network connectedness is known as *density* or *sparsity* in graph theory. The connectedness (often called ρ but symbolised with α here to avoid confusion) is given by (8) where m is the number of edges (i.e. power system branches) and k is the number of vertices (i.e., buses) in a graph [21].

$$\alpha = \frac{2m}{k(k-1)} \tag{8}$$

Variations in both shortest path length and network connectedness can be created by bringing transmission lines in/out of service in multi-area power systems.

3.6. Fast frequency response (FFR) modelling

In this subsection, the FFR controllers used in this study are presented. Given the great flexibility and controllability, grid-scale battery energy storage systems (BESSs) are considered as the FFR provider. Two types of FFR control schemes are of interest including proportional (known as *droop*) control and derivative control (known as *synthetic inertia*). The two controller structures are displayed in Fig. 3.

The input of the frequency controllers is the frequency deviation (Δf) which is the difference between nominal frequency (f_n) and locally measured frequency (f_{meas}). A dead band is implemented to prevent excessive operation of FFR around f_n. The droop controller differs

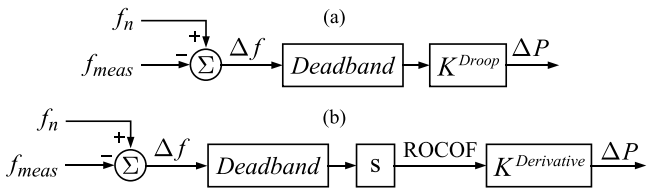

Fig. 3. Supplementary frequency controller: (a) droop controller; (b) derivative controller.
Source: Adopted from [10].

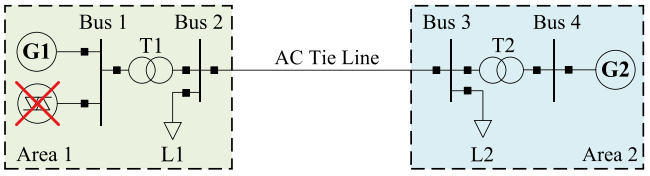

Fig. 4. Generic two-area test network.

from the derivative controller in terms of the signal that is input into the proportional gain (K^{Droop} and $K^{Derivative}$). The former acts on Δf whereas the latter acts on the rate of change of Δf (i.e., ROCOF). A basic derivative function block $F(s) = s$ is used in this research to enable inertial response emulation and the derivative is taken every time step of the simulation. It is acknowledged that designing a robust derivative controller is beyond the scope of this paper and, hence, practical difficulties associated with derivative control implementation as outlined in [23] are neglected. The output signal (ΔP) is sent to the outer active power control loop which is subjected to a ramp limiter to represent converter power ramp limitations.

4. Application & results

In this section, the details of the application of the methodology outlined in Section 3 will be presented. All modelling and simulations are performed using DIgSILENT PowerFactory with additional use of Python to automate the vast numbers of simulations. MATLAB is used to calculate the values of CS and perform correlation analysis.

4.1. Test networks

Three test networks are used to perform the analysis in this paper. The first network is a generic two-area model which is used to generate the key results in this paper. The second network is a generic four-area model which is uniquely used to enable the studies associated with topological variations to be undertaken. The third network is a reduced order dynamic GB system model. It is used to verify that the key results obtained using the small two-area model can be generalised to larger, more practically scaled power networks.

4.2. Application on a two-area network

The two-area network is shown in Fig. 4. The two areas are connected via a single AC transmission line. Each area consists of an SG and a load. The disconnection of a static generator at Bus 1 (Area 1) is used to unbalance the system.

The SGs are represented by 6th-order models with dynamic parameters selected from [24] to represent CF1-HP gas-fired generator. Both SGs use IEEE-DC1 A exciter and operate with GASTWD governor. The nominal governor droop (R) is set at 5% (20 pu droop gain). Power system stabilisers (PSSs) are not implemented to help isolate the damping of the electromechanical oscillations as inherent system properties and not supplementary damping control. System loads are

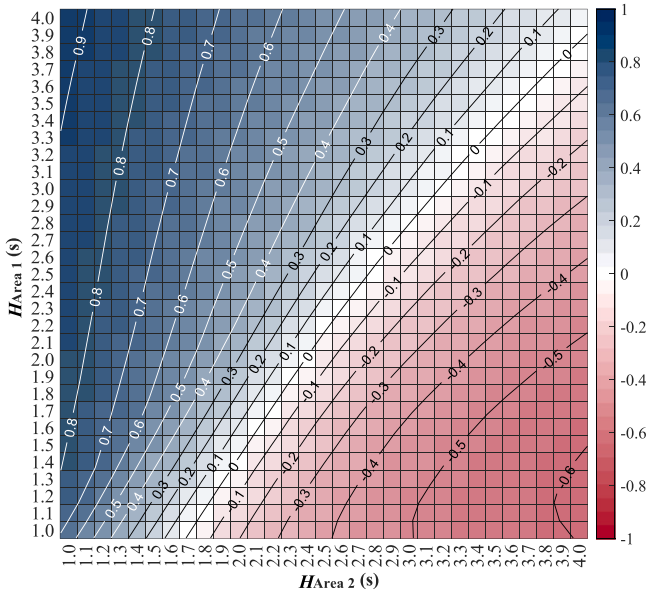

Fig. 5. Cosine similarity between regional frequency deviations.

modelled using a ZIP model with coefficients taken from [25]. The two SGs are equal in size and equally dispatched (with G2 the slack bus). The sum of loads is equivalent to the summer loading condition in the GB system (36 GW). The network initially operates with 1 GW of power transferring from Area 1 to Area 2. The disturbance is sized to 1800 MW, equivalent to the Infrequent Infeed Loss Risk for the GB system. The impedance of the single AC tie (Z_{tie}) is 2.25 + j22.5 Ω, representing the electrical distance between Scottish and English networks [26].

For different inertia distributions creation, the H values of both SGs are varied in the range [1, 4] s in 0.1 s steps. Assessing the impact of all combinations of regional inertia, leads to a total 961 simulations. The CS between the speed trajectories of the two SGs is calculated for each simulation.

4.2.1. Preliminary analysis

Preliminary analysis of the results for all scenario combinations is presented using the heat map shown in Fig. 5. The obtained 961 values of CS are laid out into a 31 × 31 matrix whose rows and columns are values of H_{Area1} and H_{Area2} respectively. Note that the values of H_{Area1} and H_{Area2} are determined on the same system base. Thus, the quantity of the total E_{syn} within a specific area can be described with respect to H and can be directly used for comparison. Cells with the same CS value are connected by contours, representing the CS value in the range [–0.6, 0.9].

The cells in the upper left of Fig. 5 represent regional inertia combinations that result in positive values of CS. Whereas the cells in the bottom right of the graph represent the combinations that result in negative CS values. For each H_{Area1} (the disturbance area), the values of CS decrease with successive increases in H_{Area2} (the non-disturbance area). The greatest variation in CS is seen when H_{Area1} is equal to 1 s (as shown by the contours). The maximum value of CS (0.934) is seen when H_{Area1} = 4 s and H_{Area2} = 1 s, whereas the minimum value of CS (–0.606) is seen when H_{Area1} = 1 s and H_{Area2} = 4 s.

4.2.2. Correlation

It can be seen from Fig. 5 that the contours are close to linear. This might indicate a regional inertia combination equivalence with respect to CS, and the ratio (Φ_H) of the disturbance area inertia (H_{Area1}) to that of the non-disturbance area (H_{Area2}) is of concern. Fig. 6(a) displays the scatter plot of the relationship between Φ_H and CS. Also included

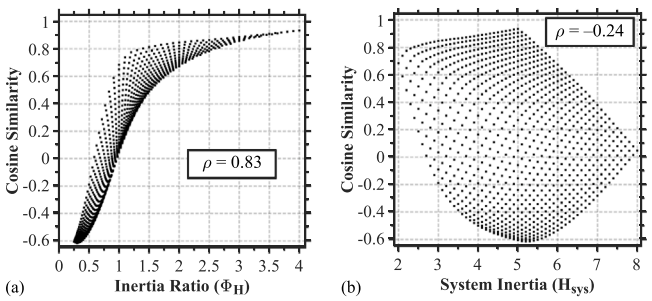

Fig. 6. Pearson correlation of cosine similarity with: (a) inertia ratio Φ_H; (b) system inertia H_{sys}.

Table 1
Regional- and system-wide inertia, Φ_H, and CS.

Case	H_{Area1}	H_{Area2}	H_{sys}	Φ_H	CS
Heterogeneous	1 s	4 s	5 s	0.25	–0.606
	4 s	1 s	5 s	4.00	0.934
Homogeneous	1 s	1 s	2 s	1.00	0.684
	4 s	4 s	8 s	1.00	0.048

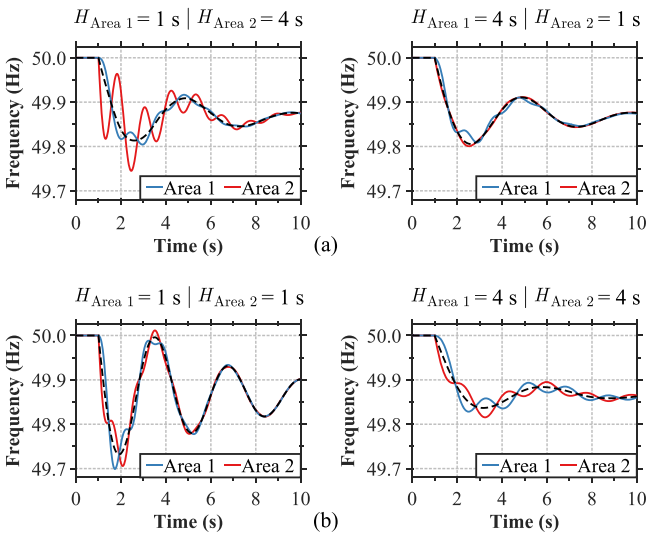

Fig. 7. Regional frequency deviations under different inertia distributions: (a) *Heterogeneous* case; (b) *Homogeneous* case.

for comparison is the relationship between H_{sys} and CS, as shown in Fig. 6(b). The correlation coefficient (ρ) is calculated for both cases.

A strong positive correlation between Φ_H and CS is seen (ρ = 0.83). Whereas no correlation is found between H_{sys} and CS (ρ = –0.24). This indicates that the extent of the localness of regional frequency is highly dependent on Φ_H, not the inertia of a specific area, nor the level of system inertia. Broadly, the two areas are highly synchronous only when Φ_H is greater than 2.5 (all values of CS are greater than 0.8). Looking back to the heat map shown in Fig. 5 alongside the scatter plot shown in Fig. 6(a), it also indicates that homogeneous inertia distributions do not demonstrate significant advantages of inhibiting frequency heterogeneity. This is particularly true when the system operates at high inertia levels.

To gain a detailed insight into the distinction in CS, four cases described in Table 1 are used. The two *Heterogeneous* cases result in the minimum and the maximum CS values respectively. The two *Homogeneous* cases are representing conditions when both areas (and hence the system) exhibit the lowest and the highest level of inertia across all scenario combinations respectively. Fig. 7 presents the transient responses.

Fig. 7(a) indicates that in the presence of heterogeneous inertia distribution, the system experiences notable variations in regional frequency only if the disturbance occurs in the low inertia area. This is because the corresponding SG will experience larger frequency deviations with respect to the high inertia area, governed by the swing equation (2). The resulting differences in regional frequency deviations thus lead to the minimum value of CS. Conversely, if the disturbance occurs in the high inertia area, then the disturbance-induced physical impact will be largely absorbed by the large rotating masses. Any difference in the regional frequency is relatively small and generator speeds vary consistently during the event. This explains the reason why the resulting value of CS is close to 1.

The transient responses shown in Fig. 7(b) highlight that homogeneous inertia distributions do not directly suggest a desirable system behaviour as persistent inter-area oscillations can be incurred when the system operates at high inertia levels. For the case when H_{sys} = 2 s, although both areas experience higher ROCOFs, the inter-area oscillation is adequately damped around 5 s after the event. When H_{sys} increases to 8 s, poorly damped but stable oscillations are seen — the transition from localness to homogeneity is comparatively slow in terms of regional frequency deviations. The smaller CS value seen in the case with H_{sys} = 8 s is hence explained.

The present results display that the inertia ratio Φ_H exhibits a strong positive correlation with CS. This is demonstrated for a single set of operating conditions with a unique governor control and network topology. To help make the results more generalisable, studies into the effects of governor control and network topology are given in the following two subsections.

4.3. Variation in SG dynamics

Within this subsection, studies into the impact of detailed disaggregated modelling of SGs and their turbine-governor controls are presented. All simulations are performed on the two-area model. For each new case study, values of CS are calculated for all 961 scenarios.

Two comparative studies will be presented. The former examines the impact of varying *governor droop* where three possible values of *R*, 3%, 5%, and 9% are considered. This is completed using the GASTWD governor identical to the previous subsection. The latter examines the impact of different variants of machines and associated *turbine-governor controls* in which a comparison is made between three types of generating units, including hydraulic, gas-fired, and nuclear. Two new case studies are hence created by entirely replacing the originally installed gas-fired units with hydro and nuclear units respectively (the machine rating remains unchanged). The hydro units are represented by H4 hydraulic generator (using 5th-order models), and the nuclear units are represented by N1 nuclear steam generator with dynamic parameters taken from [24]. Significantly, the hydro units operate with HYGOV governor, and the nuclear units operate with IEEEG1 governor. As with the GASTWD governor, the droop *R* is set to 5%. A single type of SG (and associated governor control) is used at this stage so that both SGs respond in a similar manner.

Figs. 8(a) and (b) present the scatter plots of the relationship between Φ_H and CS for the two comparative studies respectively. The correlation coefficient (ρ) is calculated for each case as before.

Fig. 8(a) provides indications of the robustness of the previously observed correlation between Φ_H and CS to variations in governor droop as little change in ρ is seen. It is noted that the scatter plots are essentially indistinguishable between different cases. This reveals that changing governor droop has a negligible impact on frequency heterogeneity. Further analysis by the authors (not included for brevity) demonstrates that increasing the governor droop improves the frequency nadir; the electromechanical interaction between SGs, however, remains largely unchanged over the same timeframe. This is consistent

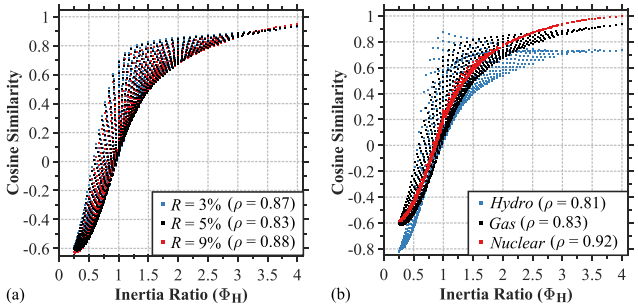

Fig. 8. Variation in SG dynamics analysis: (a) governor droop; (b) generation type and turbine-governor control.

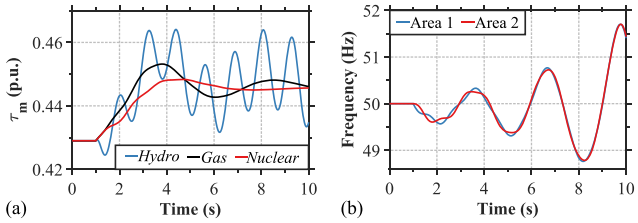

Fig. 9. Time domain responses: (a) mechanical torque (τ_m) oscillation; (b) regional frequency deviations for hydro units.

with [20] which indicates that electromechanical modes of the system are not significantly affected by changes in governor droop.

From the values of ρ in Fig. 8(b), it can be seen that the relationship between Φ_H and CS consistently exhibits a strong positive correlation when different variants of generation are incorporated. The highest correlation occurs for the *Nuclear* case, for which ρ = 0.92. For the *Hydro* case, a slight degradation in the strength of the correlation is seen (ρ = 0.81). What also stands out in Fig. 8(b) is that the scatter plot for the *Hydro* case differs from that of the other types of generation. Firstly, smaller values of CS are seen for the *Hydro* case, indicating degradation in frequency heterogeneity. An inspection of the cause reveals that the hydro units exhibit greater mechanical oscillations compared to the gas and nuclear units, as shown in Fig. 9(a). Closer inspection of the initial swing of τ_m indicates that the significant oscillatory behaviour of the hydro units might be attributed to the *non-minimum phase* characteristic of the HYGOV governor control. This comparison is generated for the case when H_{Area1} = 1 s and H_{Area2} = 4 s, in which τ_m of G1 is of interest.

Secondly, the pattern of points monotonically slopes from lower left to upper right for both *Gas* and *Nuclear* cases (though it is much tighter for the *Nuclear* case). The *Hydro* case, however, does not display such a monotony trend. The value of CS peaks at 0.876 when $H_{\text{Area1}} = H_{\text{Area2}}$ = 1 s (Φ_H = 1). It then levels off and reaches 0.732 as Φ_H increases to 4. Fig. 9(b) displays the frequency response of the hydro units for the case when $H_{\text{Area1}} = H_{\text{Area2}}$ = 1 s. Unstable oscillations are seen despite the fact that the inter-area oscillations are adequately damped. Again, such coherent but unstable oscillatory behaviour might stem from the non-minimum phase characteristic of the HYGOV governor, which ultimately leads to the unique shape of the point cloud for the *Hydro* case.

This subsection provides important insights into how different governor droops and governor controls affect the correlation between Φ_H and CS. Although the system behaves in a slightly different manner due to differences in control properties, a strong positive correlation between Φ_H and CS is always seen.

4.4. Variation in network topology

A comparative analysis is first presented to examine the impact of *shortest path length*. The two-area model is used as the test network,

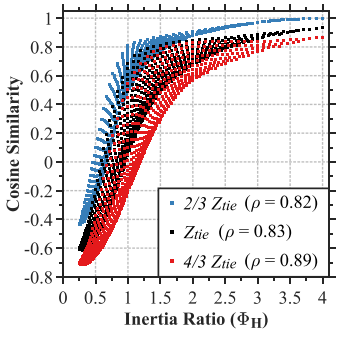

Fig. 10. Variation in shortest path length analysis.

Table 2
Connectedness of each topology.

	T1	T2	T3	T4	T5	T6
α	1.00	0.83	0.67	0.67	0.50	0.50

picking the original system setups described in Section 4.2. The electrical distance between Areas 1 and 2 is the AC tie impedance (Z_{tie}). Comparison between three possible path lengths, 2/3 Z_{tie}, Z_{tie}, and 4/3 Z_{tie}, are made, thereby two additional sets of CS values are obtained by undertaking all 961 scenarios. Fig. 10 displays the scatter plots of the relationship between Φ_H and CS. The correlation coefficient (ρ) is calculated for each case as before.

It is evident that a strong positive correlation between Φ_H and CS still exists in the presence of different path lengths. For the *4/3* Z_{tie} case, ρ = 0.89. For the *2/3* Z_{tie} case, there is a decrease in ρ (to 0.82) however this is very slight. This hence indicates the robustness of the correlation between Φ_H and CS to changes in path length. It is also evident that the values of CS are decreased as the path length increases — indicating deterioration in frequency heterogeneity. This is particularly true for the case when Φ_H is at its smallest value (0.25). For the *2/3* Z_{tie} case, the value of CS is –0.437. When the path length is doubled to *4/3* Z_{tie}, the value of CS is decreased by 61% to –0.704. Further studies by the authors (not included for brevity) show that an increase in the path length results in a reduction in the damping of the electromechanical oscillations between SGs. This can result in larger differences in regional frequency, subsequently causing deterioration in frequency heterogeneity.

Another study is carried out to explore the impact of *connectedness*. From (8), it is clear that the connectedness of a two-area network always remains fixed at 1 (m = 1, k = 2). A four-area network, which allows changes in connectedness, is hence used as the test network for this study, as shown in Fig. 11(a).

The four-area model was initially introduced in [16] for frequency stability studies. Each area in the network is connected using a single AC transmission line. All lines have the same impedance. By bringing lines in/out of service, six distinct isomorphic topologies are created, as shown in Fig. 11(b). The connectedness α for each topology is given in Table 2.

Within the four-area network, each area has the same setup as an area within the two-area model described in Section 4.2. This includes the same SG model, supplementary SG controls, load composition, and line impedances. The system loading is 36 GW as before. The SG machine rating is halved with respect to the SGs in the two-area model to allow identical levels of system-wide inertia variation. The four SGs are equal in size and equally dispatched (with G4 the slack bus). The network initially operates with substantial loads installed in Area 4. The disconnection of a static generator (again, rated at 1800 MW) always occurs at Bus 8 (Area 4). The inertia ratio Φ_H is hence calculated as the ratio of H_{Area4} to the sum of H_{Area1}, H_{Area2}, and H_{Area3}. To create different inertia distributions, the H values of the four SGs are varied in

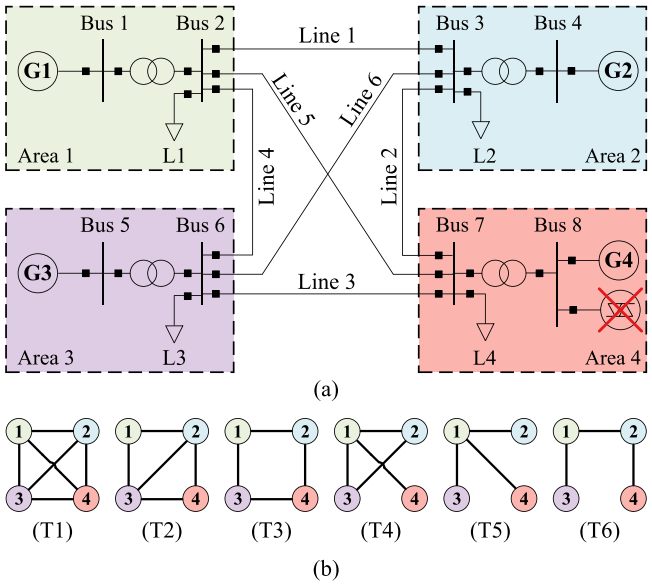

Fig. 11. (a) Generic four-area test network; (b) six isomorphic topologies for the four-area network.
Source: Adopted from [16].

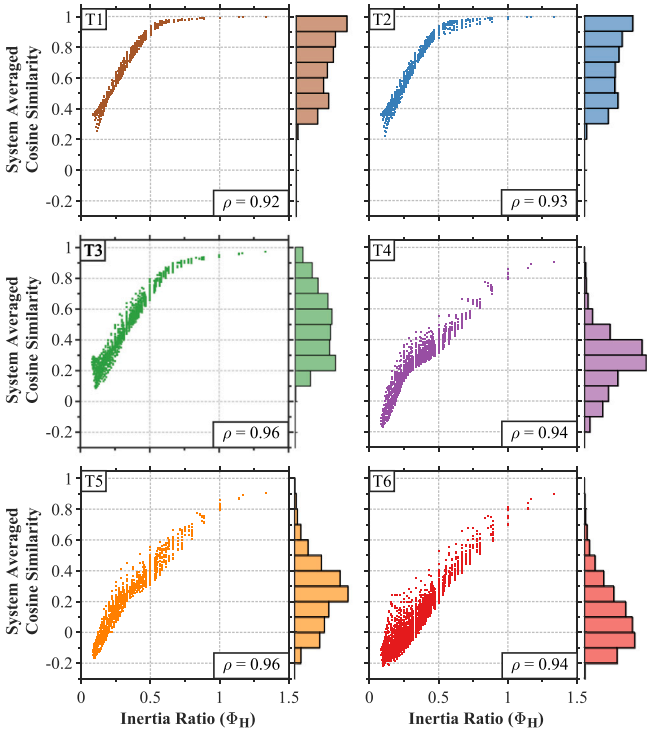

Fig. 12. Variation in network connectedness analysis.

the range [1, 4] s in 0.5 s steps. Assessing the impact of all combinations of regional inertia, leads to a total 2,401 simulations for each topology. The system averaged CS is calculated for each simulation. Fig. 12 shows the scatter plot of the relationship between Φ_H and the system averaged CS. Histograms are also included to reveal the distribution of the values of CS. Again, the correlation coefficient (ρ) is calculated for each case.

As shown in Fig. 12, the value of ρ varies in a small range of [0.92, 0.96] as the network topology changes. This indicates that the strong positive correlation between Φ_H and CS exhibits great robustness to network connectedness variations. Also, this provides some indication

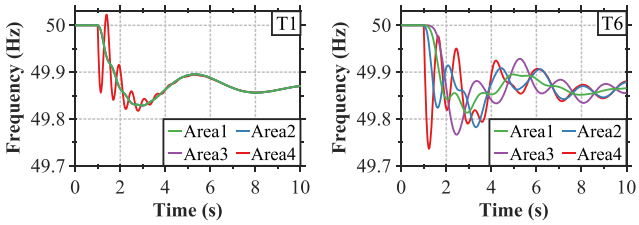

Fig. 13. Time domain comparison between topology T1 and T6.

of the generalisability of the strong positive correlation between Φ_H and CS to multi-area power systems. Another finding to emerge from Fig. 12 is that there is a gradual decrease in the values of CS as the connectedness reduces. The histograms provide further information on this finding — as the network becomes sparser, the mass of the distribution is increasingly concentrated on the bottom of the figure. To allow a deeper insight into how reduced connectedness degrades frequency heterogeneity, a time domain comparison between T1 (the fully meshed topology) and T6 (the fully radial topology) is given in Fig. 13. The results are generated for the case when Φ_H is at its smallest value (0.083).

For topology T1, the SG within the disturbance area (Area 4 in this case) is oscillating with respect to the rest of the system (Areas 1 to 3) however the oscillation is quickly damped within 3 s. Whereas for topology T6, the SGs are consistently oscillatory against each other and do not transition to a homogeneous bulk behaviour over the same timeframe.

This subsection has shown that the strong positive correlation between Φ_H and CS is capable of exhibiting good robustness with respect to network topological alterations. Extrapolating and generalising the results obtained thus far suggests that the strong positive correlation between Φ_H and CS is robust to SG dynamics and network topological alterations.

4.5. Effects of FFR on frequency heterogeneity

The previous analysis reveals that the key to being able to inhibit large variations in regional frequency is to increase the quantity of inertial energy within the disturbance area. As FFR can be considered analogous to the inertial response of SGs, this subsection will ascertain if such a rapid power injection can mitigate frequency heterogeneity. All simulations are performed on the two-area model, picking the original system setups described in Section 4.2. The BESS model in PowerFactory is implemented to represent the dynamics of the FFR devices [27]. The dead band of the frequency controllers is sized at ±15 mHz. The values of the proportional gains are taken from [28]. The ramp up limit of the BESS converter and the capacity of FFR are specified based on the technical requirements for providing the Dynamic Containment service procured by U.K. National Grid Electricity System Operator [29]. Thus, the FFR is sized to 1,400 MW, and the ramp up limit is set at 4 pu/s with respect to the BESS converter rating. It is necessary to clarify that the control scheme of the Dynamic Containment service is not implemented into the BESS, the scheme is merely used as a reference for these sizing and ramp-rate settings.

To start with, a comparative analysis is given for the two possible FFR provision locations, Areas 1 and 2, to examine how the *derivative scheme* affects frequency heterogeneity. The derivative controller described in Section 3.6 is implemented into the BESS and two sets of CS values are obtained by undertaking all 961 scenarios. Fig. 14(a) compares the scatter plot of the relationship between Φ_H and CS. Also included for comparison is the *Base case* (i.e., cases with no FFR installed).

The results shown in Fig. 14(a) indicate that the derivative controller is capable of delivering energy in the inertial timeframe and

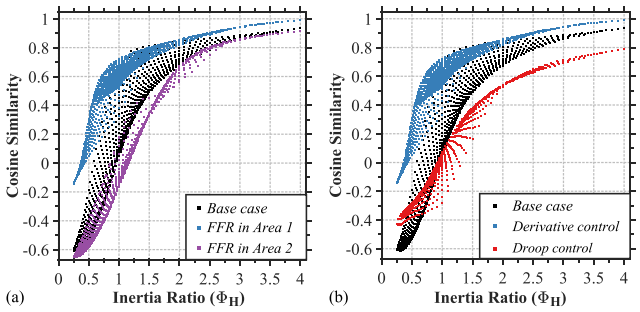

Fig. 14. Impact of FFR: (a) derivative scheme impacts on frequency heterogeneity; (b) comparison between different FFR schemes on alleviating frequency heterogeneity.

hence, affecting the frequency heterogeneity. The FFR provision in Area 1 acts to increase the inertial energy within the disturbance area and hence, larger values of CS are seen compared to when no FFR is installed. Conversely, as the FFR provision in Area 2 increases the inertial energy within the non-disturbance area, smaller values of CS are seen. These findings support the previous notion that increasing the quantity of inertial energy within the disturbance area is advantageous and improves the system performance. This, in turn, implies that providing synthetic inertia services within the non-disturbance area would risk the system stability. These results highlight the necessity of allocating inertia-like frequency containment services in areas that could be susceptible to large power in-feed losses.

Having established the applicability of the derivative control on frequency heterogeneity inhibition, another comparative study is carried out to examine the capability of the *droop scheme* to inhibit frequency heterogeneity when the service is provided within the disturbance area. The droop controller described in Section 3.6 is implemented into the BESS and again, 961 simulations are performed to obtain values of CS. Fig. 14(b) compares the scatter plot of the relationship between Φ_H and CS, the *Base case* is included as before.

For the vast majority of cases investigated, the provision of the droop based FFR leads to deterioration in frequency heterogeneity compared to when no FFR is installed. Although in some cases the values of CS are increased, the derivative scheme is always shown to provide a superior performance for frequency heterogeneity inhibition over the droop scheme. To demonstrate the difference in FFR behaviour during transients, a further comparative analysis is given. The results are generated for the case when $H_{\text{Area1}} = 1$ s and $H_{\text{Area2}} = 4$ s. Focus is paid to the impact of FFR (P_{FFR}) on τ_{net} within G1. Fig. 15 displays the transient responses. Note that occasional linear power injection is because the FFR control is subjected to a ramp limiter.

The CS value is increased to –0.142 with the derivative scheme applied (compared to –0.606 previously), whereas the CS is increased to –0.425 with the droop scheme applied. Looking back to the swing equation (2) and the derivative controller shown in Fig. 3(b), as ΔP is proportional to the ROCOF, injections of power are always delivered within the same time frame when τ_{net} is negative, as shown in Fig. 15(a). Consequently, the swings of τ_{net} are fully offset by the power injections. As shown in Fig. 15(b), although the battery starts to deliver power when the τ_{net} is negative, it is inevitable that sometimes injections of power coincide with the time when G1 experiences positive τ_{net} due to the droop controller output being proportional to Δf. The power injections hence further accelerate the rotor during each swing, aggravating the τ_{net} oscillation. This explains the reason why droop scheme provides limited benefit to the CS improvement, and sometimes has an adverse effect.

4.6. Analysis on Great Britain system

In this subsection, a reduced order model of the GB transmission system in 2030 is used to verify that the key results can be generalised. The network diagram is shown in Fig. 16. It consists of 29

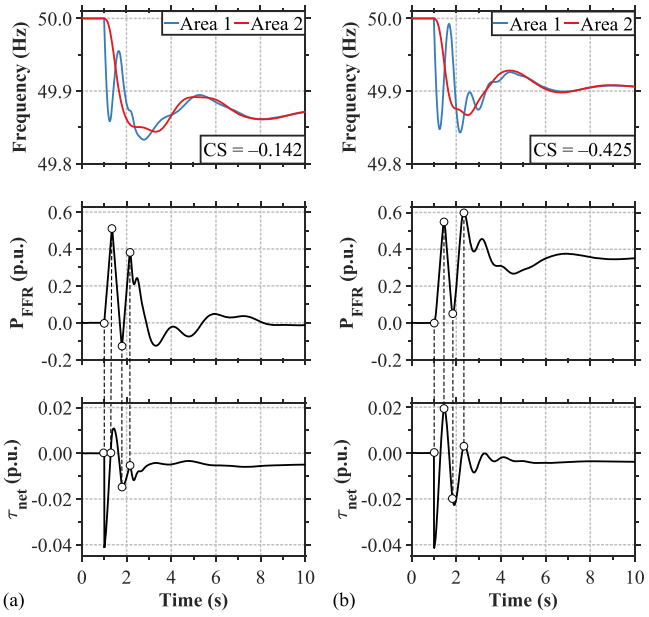

Fig. 15. Differences in FFR behaviour during transients: (a) derivative control; (b) droop control.

Table 3
Proportion of type of turbine-governor control.

HYGOV	GASTWD	WSIEG1
8.6%	46.1%	45.3%

nodes with the B6 boundary (shown in red dashed line) separating the system into two areas, Scottish and English networks. Each node in the system represents a zone that contains large amounts of loads and/or generation. High flows of power are transferred from the Scottish network to the English network, with the two areas prone to inter-area oscillations following disturbances. Five types of SG, including nuclear, CCGT, OCGT, coal, and hydro, are incorporated into the model. All SGs operate with turbine-governor controls: coal-fired and nuclear units use WSIEG1 governor (an augmented version of the IEEEG1 governor), gas-fired units use the GASTWD governor and, hydro units use the HYGOV governor. In addition, the network incorporates 3 embedded HVDC links, 15 HVDC interconnectors, and a multitude of converter-based wind power plants, representing a mixed AC/DC power system that exhibits a high level of non-linear characteristics. Both the hydro units at Nodes 1 and 3 are equipped with IEEE-PSS1A PSSs. System loads are modelled using the ZIP model as before. All CIGs within the system are operated as constant power sources and do not provide any frequency containment services. Full network details are given in [30], with further explanations of the modifications detailed in [31].

Considering summer loading (36 GW), a possible future operating scenario is created. The total E_{syn} in the system is roughly 100 GVA·s, of which 16 GVA·s are stored in the Scottish network and 84 GVA·s are stored in the English network. Table 3 outlines the proportion for each type of turbine-governor control employed in this scenario (with respect to the total installed capacity of SGs). This represents a typical SG mix of the GB system in which over 90% of the machines operate with gas and steam turbine-governor controls.

The disturbance is again implemented by disconnecting an extra static generator with the power deficit sized to 1800 MW. For clarity, *regional COI frequency* (for the Scottish and English regions) is used to represent the collective frequency dynamics of each area in the system. Frequency heterogeneity is quantified by calculating the CS between the two regional COI frequency trajectories.

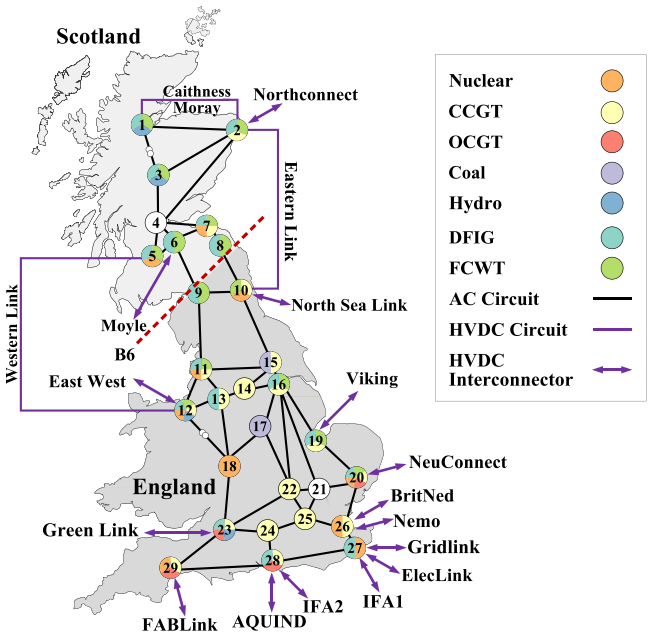

Fig. 16. Single-line diagram of 29-node GB system in 2030.

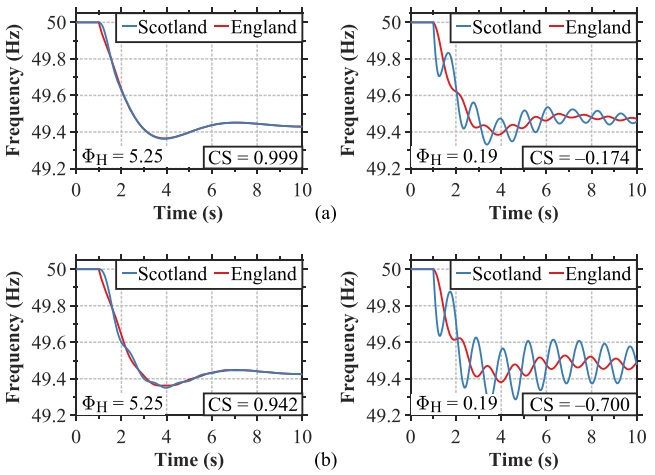

Fig. 17. Time domain comparison: (a) *Base case* scenario, (b) *Outage case* scenario.

Simulations have been performed for two cases: the *Base case* with the nominal operating conditions, and an *Outage case* with a key AC tie (the double-circuit transmission line 8–10 across the B6 boundary) removed from service. The *Base case* scenario is used to verify the impact of the inertia ratio Φ_H on frequency heterogeneity. Two inertia ratios are considered, 5.25 when the disturbance occurs in the English network, and 0.19 when the disturbance occurs in the Scottish network. Based on the previous analysis presented, we would expect the regional frequency deviations to be highly coherent when $\Phi_H = 5.25$. Conversely, the system should experience distinct regional frequencies when $\Phi_H = 0.19$. The *Outage case* scenario is used to verify the impact of increased path length on frequency heterogeneity. The double-circuit tie 8–10 provides one of the main paths for power transfer from Scotland to England. The equivalent impedance between the Scottish and English regions is hence increased when this double-circuit tie is out of service. Two inertia ratios are again considered for completeness. Generalising the previous results, it would be expected that the resulting values of CS would be reduced compared to the *Base case* scenario due to increased equivalent path length. Fig. 17 presents the transient responses for both scenarios.

As shown in Fig. 17(a), the regional frequency deviations of the two areas are nearly coincident when $\Phi_H = 5.25$, resulting in a CS value of 0.999. Conversely, notable differences in regional frequency can be seen when $\Phi_H = 0.19$, with the value of CS reduces to –0.174. These results align with the earlier observations obtained using the small two-area model: the heterogeneity of regional frequency is independent of specific regional inertia, nor of the level of system inertia. It is, in essence, highly dependent on the inertia ratio Φ_H, which, in this realistic modelling case, is dominated by the power deficit location.

The system displays deteriorating performance with respect to frequency heterogeneity when the path length between areas increases, as shown in Fig. 17(b). Consequently, the CS values are reduced compared to the *Base case* scenario. This is especially true when $\Phi_H = 0.19$, which sees a greater magnitude of regional frequency oscillations. Again, these results are consistent with the previous observations: an increase in path length can lead to deterioration in frequency heterogeneity.

5. Conclusions

This paper systematically examines how inertia distribution affects frequency heterogeneity during underfrequency disturbance events. Cosine similarity (CS) is used to quantify frequency heterogeneity. It reveals that the localness of regional frequency is largely independent of the specific area inertia and the total system inertia. The inertia ratio (Φ_H), described by the ratio of the disturbance area inertia to that of the non-disturbance area, is shown to have a strong positive correlation with CS. Regional inertia combinations that exhibit the same value of Φ_H demonstrate a similar degree of frequency heterogeneity. When the system exhibits inertia heterogeneity, the SGs are more likely to be highly synchronous if the inertia of the disturbance area is larger than that of the non-disturbance area. In view of the induced persistent inter-area oscillations, homogeneous inertia distributions do not always lead to desirable system performance. This is shown to be true when the system operates at higher inertia levels.

The observed strong positive correlation between Φ_H and CS is shown to be largely robust to widely varying conditions including turbine-governor control and network topology. Nevertheless, variations in the values of CS are seen due to differences in control system parameters and topology. Deterioration in frequency heterogeneity is seen in situations when the system is dominated by hydro power plants. This is also true when the coupling of the power network diminishes.

Providing derivative based FFR within the disturbance area is shown to improve system performance which, conversely, implies that degradation in frequency heterogeneity occurs if such a service is delivered within the non-disturbance area. From a practical context, this highlights the high value of initiating frequency event disturbance location detection. Such a scheme could potentially be used to ensure that synthetic inertia services are delivered within the disturbance area. Unlike the derivative scheme, providing droop based FFR within the disturbance area rarely demonstrates benefits to frequency heterogeneity inhibition, owing to the inevitable overlaps in time between the rapid power injection and rotor acceleration.

Overall, this paper suggests that inertia-like frequency containment services should be incorporated into areas that could be susceptible to major power deficits (e.g., large interconnector or SG in-feeds), not necessarily the areas with lower levels of inertia. A natural progression of this work is to identify regional inertia floors and regional FFR procurement limitations to ensure a reliable operation of future power systems. For example, managing regional inertia by ensuring ROCOF-related constraints may prove inadequate as the variations in locational frequency associated with small values of Φ_H can result in significant power swings and angular separation, possibly leading to instability. The inertia ratio Φ_H could be used in conjunction with angle stability metrics to produce a new stability measure for constraining the quantity of regional inertia.

CRediT authorship contribution statement

Zaichun Zhang: Conceptualisation, Methodology, Writing – original draft, Writing – review & editing. **Robin Preece:** Conceptualisation, Writing – review & editing, Supervision.

Declaration of competing interest

The authors declare that they have no known competing financial interests or personal relationships that could have appeared to influence the work reported in this paper.

Data availability

Data will be made available on request.

Acknowledgement

For the purpose of open access, the author has applied a Creative Commons Attribution (CC BY) licence to any Author Accepted Manuscript version arising.

References

[1] F. Milano, F. Dörfler, D.J. Hill, et al., Foundations and challenges of low-inertia systems (invited paper), in: 20th Power Syst. Comput. Conf., PSCC, Dublin, Ireland, 2018, pp. 1–25.
[2] D. Wilson, J. Yu, N. AlAshwal, Measuring effective area inertia to determine fast-acting frequency response requirements, Int. J. Electr. Power Energy Syst. 113 (2019) 1–8.
[3] W. Bignell, H. Saffron, T.T. Nguyen, et al., Effects of machine inertia constants on system transient stability, Electr. Power Syst. Res. 51 (1999) 153–165.
[4] A. Ulbig, T.S. Borsche, et al., Impact of low rotational inertia on power system stability and operation, IFAC Proc. Vol. 47 (3) (2014) 7290–7297.
[5] T.S. Borsche, T. Liu, D.J. Hill, Effects of rotational inertia on power system damping and frequency transients, in: 54th IEEE Conference on Decision and Control, CDC, 2015, pp. 5940–5946.
[6] A. Adrees, J. Milanović., Effect of inertia heterogeneity on frequency dynamics of low-inertia power systems, IET Gener. Transm. Distrib. 13 (14) (2019) 2951–2958.
[7] X. Cao, I. Abdulhadi, A. Emhemed, et al., Evaluation of the impact of variable system inertia on the performance of frequency based protection, in: 12th IET Int. Conf. Dev. Power Syst. Prot., 2014, pp. 1–6.
[8] A. Birchfield, Inertia adequacy in transient stability models for synthetic electric grids, in: 11th Bulk Power Systems Dynamics and Control Symposium, IREP 2022, Banff, Canada, 2022, pp. 1–8.
[9] P. Dattaray, B. Graham, et al., Identifying Regional Inertia Issues Using Graph Theory and Specitral Clustering, Tech. Rep. General Session 2022, CIGRE, 2022.
[10] J. Fradley, R. Preece, M. Barnes, VSC-HVDC for frequency support (a review), in: 13th IET Conference on AC and DC Power Transmission, ACDC, Manchester, UK, 2017, pp. 1–6.
[11] A. Venkatraman, U. Markovic, D. Shchetinin, et al., Improving dynamic performance of low-inertia systems through eigensensitivity optimization, IEEE Trans. Power Syst. 36 (5) (2021) 4075–4088.
[12] B.K. Poolla, D. Gross, F. Dörfler, Placement and implementation of grid-forming and grid-following virtual inertia and fast frequency response, IEEE Trans. Power Syst. 34 (4) (2019) 3035–3046.
[13] F. Paganini, E. Mallada, Global performance metrics for synchronization of heterogeneously rated power systems: The role of machine models and inertia, in: 55th Annu. Allerton Conf. Commun. Control Comput., 2017, pp. 324–331.
[14] P. Tielens, D.V. Hertem, The relevance of inertia in power systems, Renew. Sustain. Energy Rev. 55 (2016) (2016) 999–1009.
[15] P.V. Brogan, R.J. Best, D.J. Morrow, et al., Effect of BESS response on frequency and RoCof during underfrequency transients, IEEE Trans. Power Syst. 34 (1) (2019) 575–583.
[16] J. Fradley, R. Preece, M. Barnes, The influence of network factors on frequency stability, IEEE Trans. Power Syst. 35 (4) (2020) 2826–2834.
[17] Z. Lin, F. Wen, Y. Ding, et al., WAMS-based coherency detection for situational awareness in power systems with renewables, IEEE Trans. Power Syst. 33 (5) (2018) 5410–5426.
[18] A. Edwards, An Introduction to Linear Regression and Correlation, second ed., W.H. Freeman, 1976.
[19] J. Machowski, J. Bialek, J. Bumby, Power System Dynamics: Stability and Control, John Wiley & Sons, UK, 2020.
[20] Dynamic Models for Turbine-Governors in Power System Studies, Tech. Rep. PES-TR1, IEEE Task Force on Turbine-Governor Modeling, 2013.
[21] M. Newman, Networks: An Introduction, Oxford Univ. Press, London, UK, 2010.
[22] J.J. Grainger, W. Stevenson, Power System Analysis, McGraw-Hill, New York, US, 1994.
[23] E. Rakhshani, et al., Analysis of derivative control based virtual inertia in multi-area high-voltage direct current interconnected power systems, IET Gener. Transm. Distrib. 10 (6) (2016) 1458–1469.
[24] P.M. Anderson, A.A. Fouad, Power System Control and Stability, second ed., Wiley India Pvt. Limited, 2008.
[25] A. Tellez, Modelling Aggregate Loads in Power Systems (Master's thesis), KTH Royal Inst. of Tech., 2017.
[26] Anaya-Lara, Olimpo, Hughes, et al., Influence of windfarms on power system dynamic and transient stability, Wind Eng. 30 (2) (2006) 107–127.
[27] Application Example, Battery Energy Storing Systems, Tech. Rep., DIgSILENT PowerFactory, 2010, pp. 1–28.
[28] M. Francisco, L. Jose, Modelling and Simulation of Power Electronic Converter Dominated Power Systems in PowerFactory, Springer Press, 2020.
[29] Dynamic Containment. https://www.nationalgrideso.com/industry-information/balancing-services/frequency-response-services/dynamic-containment.
[30] S. Asvapoositkul, Data-Driven Small-Signal Stability Assessment and Preventive Control in Low Inertia Power Systems (Ph.D. thesis), Univ. of Manchester, 2021.
[31] Z. Zhang, S. Asvapoositkul, R. Preece, Impact of fast frequency response on power system transient stability, in: 17th IET Conference on AC and DC Power Transmission, ACDC, Glasgow, UK, 2021, pp. 13–18.